Available online at www.sciencedirect.com
SCIENCE DIRECT
Journal of Catalysis 229 (2005) 185–196
JOURNAL OF CATALYSIS
www.elsevier.com/locate/jcat

# Methane autothermal reforming with and without ethane over mono- and bimetal catalysts prepared from hydrotalcite precursors

Katsutoshi Nagaoka [1], Andreas Jentys, Johannes A. Lercher *

*Lehrstuhl für Technische Chemie II, Technische Universität München, Lichtenbergstr. 4, 85747 Garching, Germany*

Received 7 August 2004; revised 6 October 2004; accepted 8 October 2004

Available online 8 December 2004

**Abstract**

Autothermal reforming of methane (in the presence or absence of ethane) over Ni and/or Rh catalysts prepared from hydrotalcites is reported. Surface and bulk structures of the reduced supported metal catalysts were characterized by various physicochemical techniques. XANES and EXAFS at the Ni and Rh *K*-edges indicate that the reduction of $Ni^{2+}$ and $Rh^{3+}$ in the support matrix with $H_2$ was incomplete for all catalysts. NiRh alloy particles are formed in NiRh/MgAl. IR spectra of adsorbed CO indicate that the surface of the NiRh alloy particles is enriched in Ni. All catalysts hardly catalyzed coke formation during $CH_4$ autothermal reforming. The surface concentration of reduced Ni was critical for the catalytic activity, i.e., the catalytic activity decreased in the order NiRh/MgAl > Ni/MgAl-2 > Rh/MgAl-1. However, Ni/MgAl-2 lost its activity, when cycling between 1073 and 773 K at very high space velocities ($1.2 \times 10^4$ l/(h g)) through oxidation of metallic Ni. In contrast, NiRh/MgAl was relatively stable, while Rh/MgAl-1 did not deactivate. The enhanced stability of NiRh/MgAl by Rh against oxidation is attributed to $H_2$ spillover from Rh in the NiRh alloy as well as to its high activity (larger fraction with reducing atmosphere). The activity of all catalysts in converting hydrocarbons increased in the presence of ethane, with ethane showing a high tendency to react preferentially. Ethane could be converted completely in the presence of partly converted methane. NiRh/MgAl and Rh/MgAl-1 showed stable activity at 1073 and 773 K, while Ni/MgAl-2 gradually deactivated at 773 K. The deactivation attributed to Ni oxidation was reduced by addition of $C_2H_6$.


*Keywords:* $CH_4$ autothermal reforming; $C_2H_6$ addition; Bimetal catalyst; Hydrotalcite; NiRh alloy particles; XAS measurement; Catalytic stability; Oxidative deactivation; Coke formation

## 1. Introduction

Hydrogen based fuel cells are an attractive alternative to conventional combustion engines because of their better efficiency [1] leading in turn to a reduction of $CO_2$ emissions. Fuel cells also lower atmospheric emissions such as CO, $NO_x$, and $SO_x$. Due to the progress in fuel cell technology the demand for new catalysts to produce hydrogen increases.

Steam reforming of hydrocarbons, especially of $CH_4$, is the largest and generally the most economic way to produce $H_2$ [1–3]. However, hydrogen production for fuel cell requires high productivity, because the reformer has to be as compact as possible [4]. As a consequence, the reforming catalyst must work at very high space velocities. Thus, for breakthrough applications the catalysts must possess substantially higher catalytic activity than conventional reforming catalysts.

$CH_4$ autothermal reforming with $H_2O$ and air is a good option for reforming fuel for fuel cells feeds, as it avoids the necessity of large external supply of heat, and the cost of

* Corresponding author. Fax: +49 (0)89 289 13544.
*E-mail addresses:* nagaoka@cc.oita-u.ac.jp (K. Nagaoka), andreas.jentys@ch.tum.de (A. Jentys), johannes.lercher@ch.tum.de (J.A. Lercher).
[1] Present address: Department of Applied Chemistry, Faculty of Engineering, Oita University, Dannoharu 700, Oita 870-1192, Japan.

0021-9517/$ – see front matter 
doi:10.1016/j.jcat.2004.10.006

oxygen/nitrogen separation can be avoided for this application.

However, in contrast to the large-scale use of reformers under the typical operating conditions, reaction temperatures are varied frequently at startup and shutdown of the operation. Thus, catalysts must be able to withstand multiple cycles under those conditions and must also tolerate operation under such unusual transient conditions without deterioration. Additionally, it should be mentioned that natural gas is a regionally varying feedstock and may contain some light paraffins [1]. These are more reactive than $CH_4$ and tend to form coke rapidly [5]. In large units, an additional step (prereforming) is being introduced serving mainly to remove the heavier hydrocarbons [6]. This is impractical for small-scale reformers and hence suitable catalysts also have to tolerate mixed feeds.

Highly dispersed metals show very high and stable activity for $CH_4$ reforming [7]. In this context, Takehira et al. [7] reported that fine Ni particles can be prepared by using precursors containing $Ni^{2+}$ cations in a crystalline precursor material, which was calcined at high temperatures ($\geqslant$ 1123 K) and reduced. In that process, Ni cations homogeneously dispersed in crystalline mixed oxide, such as perovskite, were reduced and fine and stable Ni particles were formed. A similar idea has been proposed by Vaccari et al. in the preparation of hydrotalcite-like compounds (HTlcs) containing noble metals as precursor for a catalyst for the partial oxidation of $CH_4$ to synthesis gas [8]. Fine Rh particles were formed by reduction of well-dispersed Rh cations in the spinel phase. Both groups applied mono- and bimetallic catalysts prepared from HTlcs, in which metals were parts of the supports, to partial oxidation [4,9–16] as well as steam [17], $CO_2$ [9,14,18] and autothermal (i.e., the combination of partial oxidation and steam reforming) [4] reforming of $CH_4$. Among the catalysts explored NiRh showed very high activity for $CH_4$ reforming [12,14]. However, the characterization of the catalysts reported was insufficient for fully rationalizing the observations. In addition, the steady state testing of catalysts only tests part of the catalyst properties (as will be shown here) and the catalytic activity must be evaluated in multiple cycles for simulating the use of the catalysts in compact reformers.

In this contribution, we report therefore $CH_4$ autothermal reforming with or without $C_2H_6$ over mono- (Ni/MgAl and Rh/MgAl) and bimetallic (NiRh/MgAl) catalysts prepared from HTlcs followed by calcination and reduction. Various physico-chemical techniques were applied to characterize the bulk and surface structures of these catalysts and their potential reduction and oxidation. $CH_4$ autothermal reforming was carried out at extremely high space velocities ($SV = 1.7 \times 10^2$–$1.2 \times 10^4$ l/(h g)) at a cycle of temperature (1073–773–1073 K) or at constant temperature. Note that a composition of the reactants, i.e., $CH_4/O_2/Ar/H_2O = 2/1/4/2$, was used by assuming the total conversion of CO, which deactivates PEFC, to $CO_2$ in the whole catalytic reactions including shift reaction and preferential CO oxidation.

## 2. Experimental

### 2.1. Preparation of catalyst

Mono- and bimetal catalysts were prepared by using HTlcs as precursors. $[Mg_4Al_2(OH)_{12}CO_3{}^{2-}] \times 4H_2O$ was used as the base HTlc and a part of $Mg^{2+}$ and $Al^{3+}$ was replaced by $Ni^{2+}$ and $Rh^{3+}$, respectively. Compositions of catalysts are compiled in Table 1. The HTlcs were prepared by co-precipitation at room temperature by adding simultaneously a solution containing the metal nitrates and a solution containing NaOH and $Na_2CO_3$ to distilled water [19]. The pH was kept between 9 and 10 by adjusting the addition of the metal salts and base solution. The precipitates were kept in suspension under stirring at room temperature for overnight, and then filtered, washed with distilled water and dried overnight at 363 K. All samples prepared were confirmed to have typical HTlc structures by XRD analysis. These samples were calcined at 1173 K for 5 h, which completely destroys the HTlc structure and in turn forms oxide (MgO) and spinel ($MgAl_2O_4$) phases, in which Ni and Rh are dispersed homogeneously [8–10]. The powders obtained were pressed into pellets, crushed and sieved to particle sizes between 160 and 224 μm. The compositions of the catalysts after the calcination were determined by atomic absorption spectroscopy (AAS).

Table 1
Physicochemical properties of catalysts

| Catalyst | Composition[a] | Loading (wt%) | | BET surface area[b] | $H_2$ uptake | Metal dispersion[c] | Crystal size of Ni[d] |
|---|---|---|---|---|---|---|---|
| | | Ni | Rh | ($m^2/g_{cat}$) | (μmol/$g_{cat}$) | (%) | (nm) |
| Ni/MgAl-1 | Ni/Mg/Al = 6.5/61/33 | 8.3 | | 121 | 17 | 2.4 | 8.3 |
| Ni/MgAl-2 | Ni/Mg/Al = 23/44/33 | 26 | | 115 | 85 | 4.1 | 8.3 |
| NiRh/MgAl | Ni/Rh/Mg/Al = 22/0.45/44/33 | 25 | 0.89 | 109 | 142 | 6.5 | 6.6 |
| Rh/MgAl-1 | Rh/Mg/Al = 0.34/67/33 | | 0.80 | 136 | 2.4 | 6.2 | |
| Rh/MgAl-2 | Rh/Mg/Al = 0.67/65/34 | | 1.6 | n.d. | 3.5 | 4.5 | |

[a] Determined by AAS for catalysts after calcination at 1173 K.
[b] Calcined at 1173 K.
[c] Determined by $H_2$ uptake on the catalysts.
[d] Determined by using XRD results.

### 2.2. Catalyst characterization

The BET surface area was measured using a PMI automated BET-sorptometer at 77.3 K using nitrogen as analysis gas.

Transmission electron microscopy (TEM) measurements were carried out on a JEM-2010 Jeol with an accelerating voltage of 120.0 keV, equipped with a 1024 × 1024 pixel cooled slow-scan CCD-camera. Reduced catalysts, stored in air, were suspended in ethanol and ultrasonically dispersed. Drops of the dispersions were applied on a cooper grid-supported carbon film.

Metal dispersions were determined by static equilibrium adsorption of $H_2$ at room temperature using the pulse method. 100–300 mg of calcined catalysts was loaded in tubular quartz reactor (i.d. 4 mm), reduced in $H_2$/Ar (1/19, total flow rate of 60 ml/min, 10 K/min) at 1073 K for 1 h and purged with He to remove hydrogen atoms on the catalysts. After the catalysts were cooled to room temperature, doses of 0.2 ml $H_2$ were pulsed on the catalysts. The uptake of $H_2$ was measured by the mass spectrometry (MS) and the metal dispersion was calculated by assuming each metal site chemisorbs one hydrogen atom.

50 mg of the calcined catalysts was used for TPR. The calcined catalysts were heated up to 1123 K with a heating rate of 3 K/min in $H_2$/He (1/19, total flow rate of 60 ml/min) and $H_2$ uptake was measured.

100 mg of the fresh catalysts was used for TPO. After the $H_2$ reduction at 1073 K for 1 h, the catalysts were cooled to room temperature in flowing He. Then, TPO was performed in $O_2$/He (1/19, total flow rate of 60 ml/min) up to 1073 K with a heating rate of 10 K/min and $O_2$ uptake was recorded by MS.

The amount of coke deposited on the catalysts was also quantified by TPO. For that, used catalysts (containing sometimes SiC used for dilution) were transferred to the tubular quartz reactor. $O_2$/He (1/19, total flow rate of 60 ml/min) was fed to the reactor and the catalysts were heated from 300 K to 1123 K with 10 K/min. The coke deposited was oxidized to CO and/or $CO_2$ and detected by MS. For quantitative calibration of evolved $CO_2$, decomposition of $NaHCO_3$ to $CO_2$, $Na_2CO_3$, and $H_2O$ was used. TPO was also performed for SiC and fresh catalysts (before $H_2$ reduction) without SiC. The intensity of the peak for CO ($m/e = 28$) was in agreement with the fragmentation of $CO_2$ ($m/e = 44$) for all TPO experiments indicating that carbonaceous species were converted to $CO_2$. Thus, only the peaks of $CO_2$ were integrated for determining the concentrations of coke.

The XRD patterns of the catalysts were collected in Philips X'Pert-1 XRD powder diffraction-meter using Cu-$K_\alpha$ radiation. The Ni crystallite size was calculated from line broadening using the Scherrer equation [20].

IR spectra of CO adsorbed on the catalysts were measured using a Bruker IFS 88 spectrometer equipped with a vacuum cell. Fresh catalysts were reduced in $H_2$ ex situ at 1073 K for 1 h. The reduced samples were prepared as self-supporting wafers, placed into a stainless-steel cell with CaF windows, and reduced at 723 K for 2 h in a flow of $H_2$ (0.1 mbar). After the samples were cooled to 303 K in vacuum, CO (3 μbar) was flown into the cell and the spectrum was collected every 1 min for 60 min. To compare the spectra of the catalysts directly, the spectra were normalized by the weight of the wafers.

X-ray absorption spectra were measured at HASYLAB, DESY (Hamburg, Germany) on beam line X1 using the Si(111) monochromator. Higher order reflections were excluded by detuning the second crystal of the monochromator to 60% of the maximum intensity. Fresh catalysts were reduced in $H_2$ ex situ at 1073 K for 1 h and cooled down to room temperature. The reduced samples were prepared as self-supporting wafers having a total absorption of 2.5, reduced in $H_2$ in situ at 823 K for 2 h and measured at liquid $N_2$ temperature. The spectrum of the corresponding metal foil was recorded simultaneously between the second and third ionization chamber to calibrate the energy alignment of the monochromator. X-ray absorption spectra were recorded at the Ni $K$-edge (8333 eV) and the Rh $K$-edge (23220 eV) and analyzed with the program Viper [21]. The local environment of the Ni and Rh atoms was determined from the EXAFS using phase-shift and amplitude functions for Ni–O and Ni–Ni as well as Rh–Rh, Rh–O, and Rh–Ni calculated assuming multiple scattering processes (FEFF Version 8.10) [22,23].

### 2.3. Kinetic measurements

Catalyst weight was set to 10 mg diluted with 400 mg of SiC or 100 mg and loaded into a tubular quartz reactor (i.d. 6 mm). The reactor was operated in downflow mode with the catalyst bed held between quartz wool plugs. After the catalysts were reduced in situ in $H_2$ at 1073 K for 1 h followed by Ar purge, a $CH_4/O_2/Ar/H_2O$ mixture ($CH_4/O_2/Ar/H_2O = 2/1/4/2$, SV = 172.8, 1728 or 12420 l/(h g)) or a $CH_4/C_2H_6/O_2/Ar/H_2O$ mixture ($CH_4/C_2H_6/O_2/Ar/H_2O = 1.6/0.2/1/4.2/2$, SV = 1728 l/(h g)) was passed over the catalyst. A thermocouple was placed at the outside of the reactor and used to control the oven temperature. A cold trap was attached between the exit of the reactor and gas chromatograph (GC) to remove water from the educts. The reaction products were analyzed by the gas chromatograph (Hewlett Packard, HP 58901) with two capillary columns (MS-5A and Pora Plot Q) and a thermal conductivity detector (TCD). Hydrocarbon conversion was calculated with carbon balance, as the amount of coke deposited was very small to negligible. After the reaction, the catalysts were cooled to room temperature in Ar and used for further characterization.

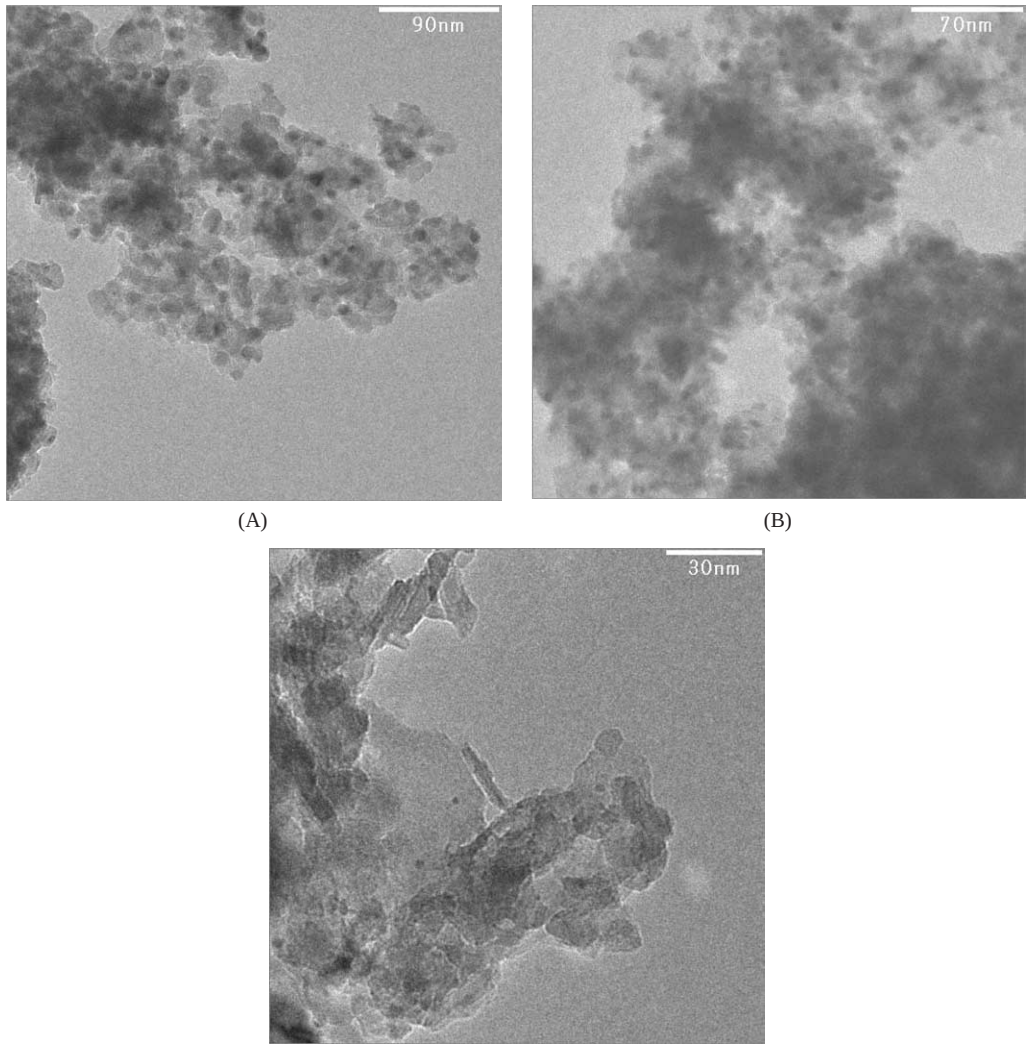


(A) (B)

(C)

Fig. 1. TEM images of (A) Ni/MgAl-2, (B) NiRh/MgAl, and (C) Rh/MgAl-1 after $H_2$ reduction at 1073 K.

## 3. Results

### 3.1. Physico-chemical property of catalysts

Metal composition, BET surface area, metal dispersion, and Ni crystal size are compiled in Table 1. All catalysts showed high BET surface areas after calcination at 1173 K. The fraction of metals exposed was below 10% for all materials prepared. On the other hand, the presence of relatively small metal particles was confirmed by XRD and TEM images (Fig. 1). The variations in the particle sizes are subtly reflecting the harsh conditions these materials were pretreated. It should be noted, however, that these small variations have a profound impact on the total concentration of metal atoms available. Note that the fraction of available metal atoms increases by 170% as Rh was added to the Ni catalysts. For the monometal catalysts, the Ni dispersion increased with increasing Ni loading, while the Rh dispersion decreased with increasing Rh loading.

In order to understand the subtle variations better two of the higher dispersion monometallic catalysts, Ni/MgAl-2 and Rh/MgAl-1, and one bimetal catalyst, NiRh/MgAl, were characterized in depth.

### 3.2. Ni XANES and EXAFS

The XANES at the Ni $K$-edge of Ni/MgAl-2 and NiRh/MgAl after reduction in $H_2$ are compared with that of Ni foil and NiO in Fig. 2. For both catalysts the intensity of the peak above the edge slightly increased compared to the metal foil, which is attributed to the presence of some Ni oxide. This suggests that the reduction of Ni cations in the support matrix is incomplete after treatment in $H_2$ at 1073 K.

The Fourier transformed EXAFS ($k^2$-weighted) at the Ni $K$-edge of the Ni containing catalysts after reduction in $H_2$, of Ni foil and of NiO are shown in Fig. 3. The results of the EXAFS analysis are summarized in Table 2. Small contributions of Ni–O ($N_{\text{Ni–O}} = 1.3$) and large contributions of Ni–Ni ($N_{\text{Ni–Ni}} = 9.2$–$9.4$) were observed for both catalysts.

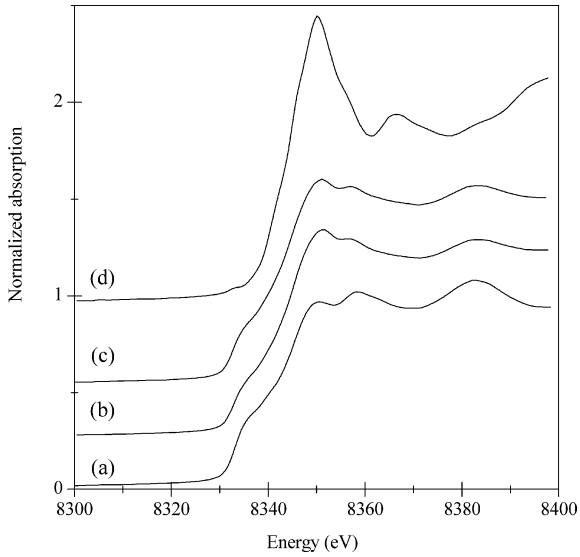


Fig. 2. Ni $K$-edge XANES for (b) NiRh/MgAl and (c) Ni/MgAl-2 after in situ $H_2$ reduction at 823 K following ex situ $H_2$ reduction at 1073 K. (a) Ni foil and (d) NiO included as references.

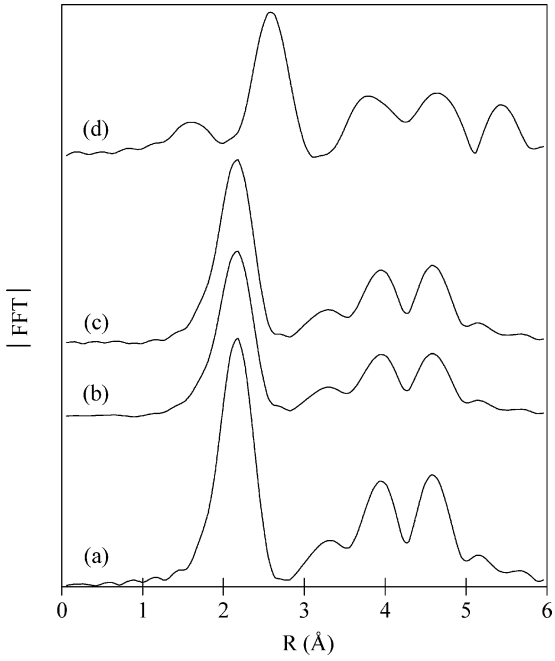


Fig. 3. Magnitude of the Fourier transformed oscillations ($k^2$-weighted) at the Ni $K$-edge of (b) NiRh/MgAl and (c) Ni/MgAl-2 after in-situ $H_2$ reduction at 823 K following ex-situ $H_2$ reduction at 1073 K. (a) Ni foil and (d) NiO included as references.

This is in agreement with the variations in the XANES and confirms that after reduction Ni is present in these catalysts in metallic and in cationic form.

### 3.3. Rh XANES and EXAFS

The XANES at the Rh $K$-edge of Rh/MgAl-1 and NiRh/MgAl after $H_2$ reduction, Rh foil and $Rh_2O_3$ are compared in Fig. 4. Similarly to the XANES observed at the

Table 2
Coordination parameters for Ni containing samples determined by X-ray absorption spectroscopy

| Sample | Ni–O | | | Ni–Ni | | |
|---|---|---|---|---|---|---|
| | $N$ | $R$ (Å) | $\Delta\sigma^2$ (Å$^2$) | $N$ | $R$ (Å) | $\Delta\sigma^2$ (Å$^2$) |
| Ni foil | | | | 12 | 2.49 | |
| NiO | 6 | 2.07 | | 12 | 2.94 | |
| Ni/MgAl-2 | 1.3 | 2.05 | 0.0081 | 9.4 | 2.49 | 0.0043 |
| NiRh/MgAl | 1.3 | 2.05 | 0.0095 | 9.2 | 2.48 | 0.0050 |

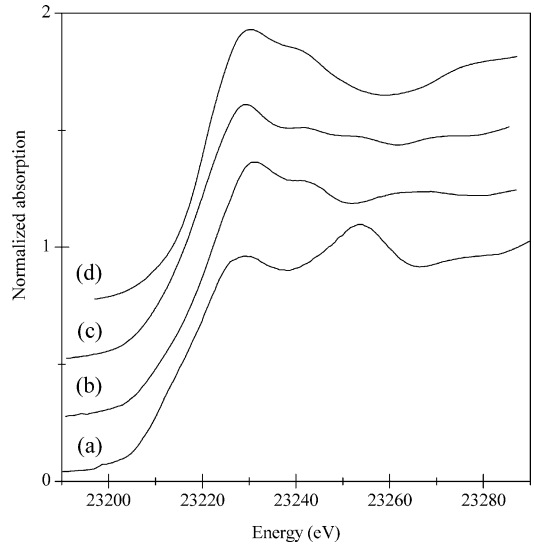


Fig. 4. Rh $K$-edge XANES for (b) NiRh/MgAl and (c) Rh/MgAl-1 after in situ $H_2$ reduction at 823 K following ex situ $H_2$ reduction at 1073 K. (a) Rh foil and (d) $Rh_2O_3$ included as references.

Ni $K$-edge an increase in the peak above the absorption edge was observed for both catalysts, which suggests the co-existence of Rh metal and Rh oxide species in the catalyst samples.

The magnitude of the Fourier transformed EXAFS ($k^2$-weighted) at Rh $K$-edge of the catalysts containing Rh after reduction is compared with Rh foil and $Rh_2O_3$ in Fig. 5. For Rh/MgAl-1, the maxima between 1–2 and 2–3 Å are assigned to Rh–O and Rh–Rh contributions, respectively. For NiRh/MgAl the contribution of the O neighbors (at 1–2 Å) was also observed, while maximum characteristic for the Rh–Rh contributions (at 2–3 Å) was smaller. In addition, a contribution at around 1.5–2.5 Å was observed, which is attributed to Rh–Ni contributions. The results of the analysis of the EXAFS at Rh $K$-edge are summarized in Table 3. Contributions of Rh–Ni, Rh–Rh and Rh–O were taken into account for analyzing the EXAFS of NiRh/MgAl.

The results clearly indicate the absence of Rh–Rh contribution and the formation of Rh–Ni neighbors in NiRh/MgAl, providing clear evidence for the formation of NiRh alloy particles. Since $N_{Rh–Ni}$ was significantly smaller than 12, we speculate that at least part of Rh is enriched at the surface of the bimetallic particles.

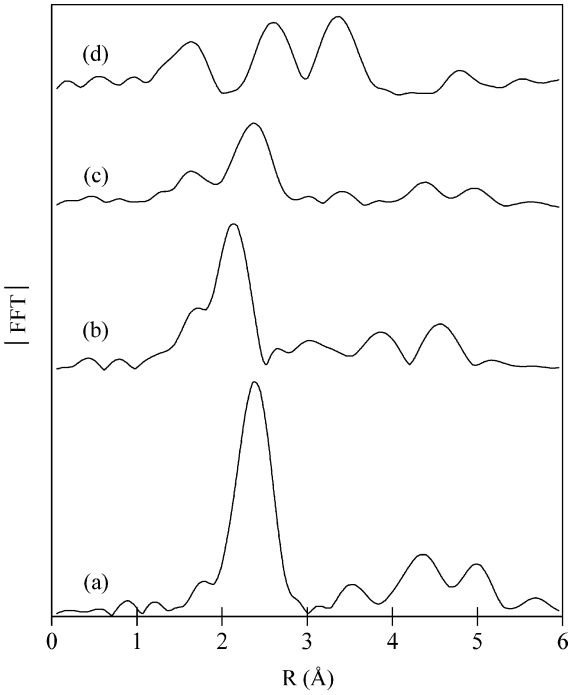


Fig. 5. Magnitude of the Fourier transformed oscillations ($k^2$-weighted) at the Rh $K$-edge of (b) NiRh/MgAl and (c) Rh/MgAl-1 after in situ $H_2$ reduction at 823 K following ex situ $H_2$ reduction at 1073 K. (a) Rh foil and (d) $Rh_2O_3$ included as references.

Table 3
Coordination parameters for Rh-containing samples determined by X-ray absorption spectroscopy

| Sample | Rh–O | | | Rh–Rh | | | Rh–Ni | | |
|---|---|---|---|---|---|---|---|---|---|
| | $N$ | $R$ (Å) | $\Delta\sigma^2$ (Å$^2$) | $N$ | $R$ (Å) | $\Delta\sigma^2$ (Å$^2$) | $N$ | $R$ (Å) | $\Delta\sigma^2$ (Å$^2$) |
| Rh foil | | | | 12 | 2.68 | | | | |
| $Rh_2O_3$ | 6 | 2.06 | | | | | | | |
| Rh/MgAl-1 | 5.3 | 2.11 | 0.0087 | 2.5 | 2.68 | 0.0017 | | | |
| NiRh/MgAl | 2.9 | 2.05 | 0.0029 | 0.1 | 2.61 | 0.0090 | 7.1 | 2.52 | 0.0041 |

### 3.4. IR spectra of adsorbed CO

To confirm the existence of Rh on the surface of metal particles of NiRh/MgAl, the metal surface was probed by adsorption of CO followed by IR spectroscopy. The IR spectra of CO adsorbed at 3 μbar on reduced Ni/MgAl-2, NiRh/MgAl and Rh/MgAl-1 are shown in Fig. 6. Two CO stretching bands were observed in the IR spectra of all catalysts. The bands at higher wavenumbers, i.e., 2000–2100 cm$^{-1}$ for Ni containing catalysts and 1910–2080 cm$^{-1}$ for Rh/MgAl-1, are ascribed to linearly adsorbed CO, while the bands at lower frequency, i.e., 1800–2000 cm$^{-1}$ for Ni containing catalysts and 1800–1910 cm$^{-1}$ for Rh/MgAl-1, are assigned to bridged bonded CO [25,26]. All bands increased with time of exposure and the bands of bridged bonded CO on Ni containing catalysts shifted slightly to higher wavenumbers. The intensities of the CO stretching bands indicate that with Ni/MgAl-2 the concentration of

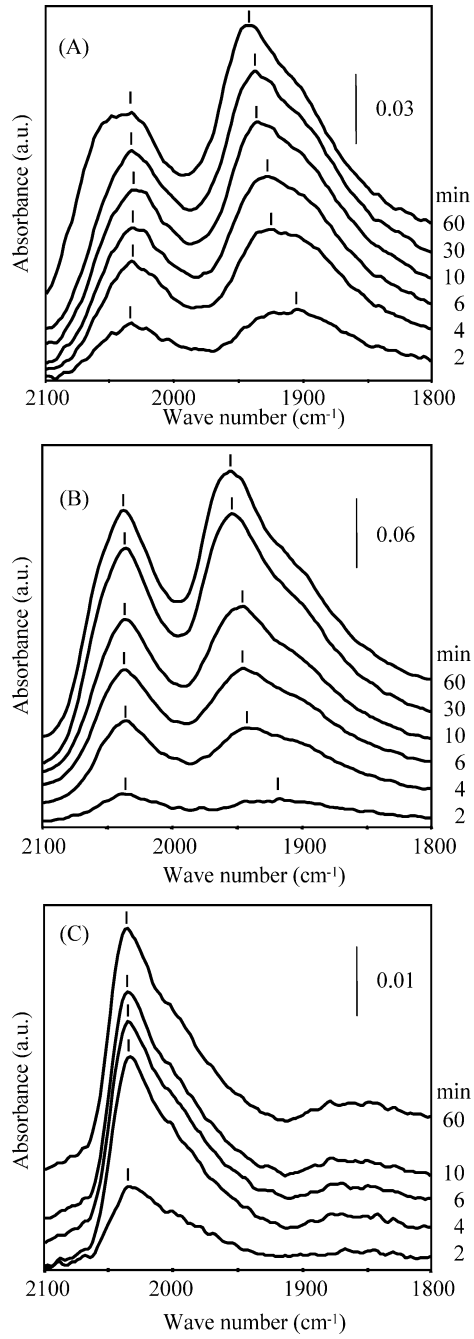


Fig. 6. IR spectra of CO adsorbed on (A) Ni/MgAl-2, (B) NiRh/MgAl, and (C) Rh/MgAl-1.

bridged bonded CO was higher than that of linearly adsorbed CO. In contrast, linearly adsorbed CO was more abundant on Rh/MgAl-1. For NiRh/MgAl, linearly bounded CO was also more abundant than bridged bonded CO at the start of exposure (2–4 min), while the ratio reversed after some time.

### 3.5. Temperature programmed reduction and temperature programmed oxidation

The behavior of the supported metals during reduction and oxidation was studied by TPR and TPO. The TPR pro-

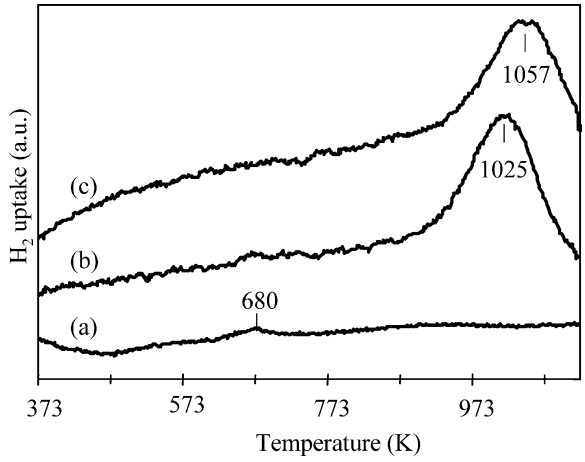


Fig. 7. TPR profiles of (a) Rh/MgAl-1, (b) NiRh/MgAl, and (c) Ni/MgAl-2 calcined at 1173 K (3 K/min).

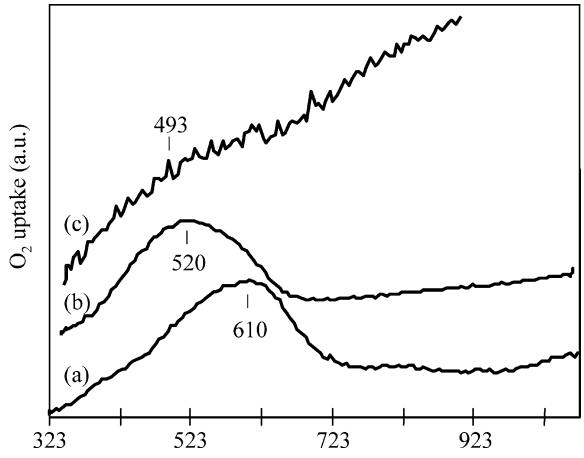


Fig. 8. TPO profiles of (a) Ni/MgAl-2, (b) NiRh/MgAl, and (c) Rh/MgAl-1 ×5 reduced at 1073 K (10 K/min).

files of Ni/MgAl-2, NiRh/MgAl and Rh/MgAl-1 calcined at 1173 K are shown in Fig. 7. The TPR profile of Ni/MgAl-2 had a single maximum at 1057 K. The high temperature required for reduction indicates that $Ni^{2+}$ is well separated in the precursor [4]. Reduction of oxidized Rh, on the other hand, had a maximum rate at 680 K. It was reported previously that Rh oxide species distributed in a precursor matrix are reduced over a wide temperature range (573–1273 K). Complete reduction of Rh with $H_2$ was achieved after 4 h at 1023 K [15]. A rough estimate of the amount of Rh reduced below 1123 K indicates that it would be too small to be detected. The maximum of the reduction of Ni oxide in NiRh/MgAl was observed at 1025 K, about 30 K lower than the reduction of Ni in Ni/MgAl-2. In this context, it is noted that $H_2$ consumption during the $H_2$ reduction was slightly higher on NiRh/MgAl than on Ni/MgAl-2. All these observations suggest that the addition of small amount of Rh promotes the reduction of Ni oxide species.

The TPO profiles of Ni/MgAl-2, NiRh/MgAl and Rh/MgAl-1 after the $H_2$ reduction are compared in Fig. 8. Rh/MgAl-1, NiRh/MgAl and Ni/MgAl-2 showed peaks at 493, 520, and 610 K, respectively. Thus, also the rate of oxidation of Ni in NiRh/MgAl increased in the presence of Rh.

### 3.6. Activity of catalysts for $CH_4/O_2/Ar/H_2O$ conversion in a temperature cycle

The catalytic activity was studied in a temperature cycle, where the oven temperature was once decreased from 1073 K to 773 K, and then increased again from 773 to 1073 K. The space velocities were adjusted to $1.2 \times 10^4$, $1.7 \times 10^3$ or $1.7 \times 10^2$ l/(h g). It should be noted that an additional thermocouple in the reactor showed significantly lower values compared to oven temperatures at very high space velocities of $1.2 \times 10^4$ l/(h g), in the absence of chemical reactions. Note that oven temperatures of 1073, 973, 873 and 773 K corresponded to 973, 873, 773 and 673 K inside the reactor. This is attributed to the very high linear velocity of the reactants (122 cm/s) under these conditions. $CH_4$ conversions of catalysts with different space velocities (SVs) are shown as a function of time in Fig. 9. Note that blank test with SiC did not show methane conversion. At the space velocity of $1.7 \times 10^3$ l/(h g), NiRh/MgAl had the highest stable $CH_4$ conversion (Fig. 9B). Among the monometallic catalysts, Ni/MgAl-2 had the highest initial $CH_4$ conversion, but lost 10% of its initial value after the temperature cycle. This led to comparable activity observed with Rh/MgAl-1. In contrast, Ni/MgAl-1 showed only very low $CH_4$ conversion from the beginning of the reaction. After the reaction, the deactivated catalysts had a greenish color pointing to oxidized Ni. The two Rh containing catalysts showed comparable and stable activity at all temperatures. The $CH_4$ conversion over NiRh/MgAl at 773 K exceeded the thermodynamic equilibrium for methane autothermal reforming. This is attributed to the preferential combustion over reforming at the lower temperature. The exothermic process would lead to a higher temperature in catalyst layer and in turn to a higher conversion.

Activity tests of Ni/MgAl-1, whose activity was rather low at a space velocity of $1.7 \times 10^3$ l/(h g), were carried out at a lower SV of $1.7 \times 10^2$ l/(h g) (see Fig. 9C). Under these conditions, the catalyst showed a high and stable $CH_4$ conversion uo to 873 K, while the activity was completely lost at 773 K. Once deactivated, the catalyst also showed only low activity at 973 K, and the $CH_4$ conversion was restored only up to 68% (71% of initial value) at 1073 K followed by slight increase to 74% with time on stream at this temperature. The color of the used catalyst was greenish at the inlet and gray at the outlet.

Catalytic activity of Ni/MgAl-2, NiRh/MgAl and Rh/MgAl-1 is compared at the very high SV of $1.2 \times 10^4$ l/(h g) (Fig. 9A). NiRh/MgAl had the highest $CH_4$ conversion among the catalyst under the used set of reaction conditions. After completing one temperature cycle, the $CH_4$ conversion at the oven temperature of 1073 K was slightly lower (90% of the initial value) than with the fresh material. Note that Rh/MgAl-1 did not show any signs of deactivation at

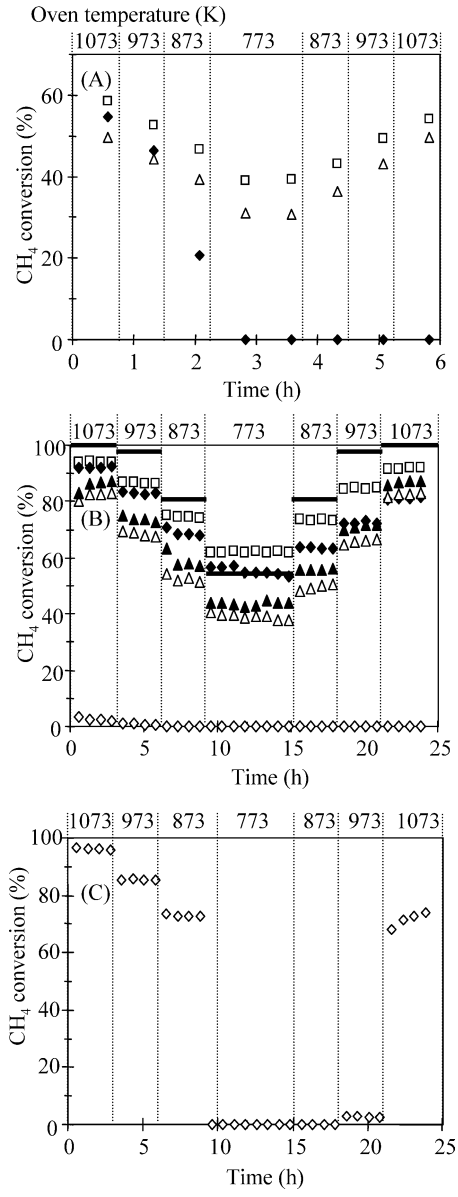


Fig. 9. $CH_4$ conversions vs time on stream for catalysts with SV of (A) $1.2 \times 10^4$, (B) $1.7 \times 10^3$, and (C) $1.7 \times 10^2$ l/(h g) (reaction condition: $CH_4/O_2/Ar/H_2O = 2/1/4/2$). Solid lines in (B) show equilibrium $CH_4$ conversion at each temperature. (◇) Ni/MgAl-1, (◆) Ni/MgAl-2, (□) NiRh/MgAl, (△) Rh/MgAl-1, (▲) Rh/MgAl-2.

1073 K. In contrast, the activity of Ni/MgAl-2 was completely lost at 773 K and was not recovered, even if the temperature was increased to 1073 K. The color of the used Ni/MgAl-1 was green, whereas that of the other catalysts was gray.

### *3.7. Activity of and coke deposition on catalysts for $CH_4/O_2/Ar/H_2O$ conversion at constant temperature*

Activities and stabilities of Ni/MgAl-2, NiRh/MgAl and Rh/MgAl-1 were tested at 1073 K and 773 K, and the results are presented in Fig. 10. The SV was fixed to $1.7 \times 10^3$ l/(h g) in these experiments. Note that blank test

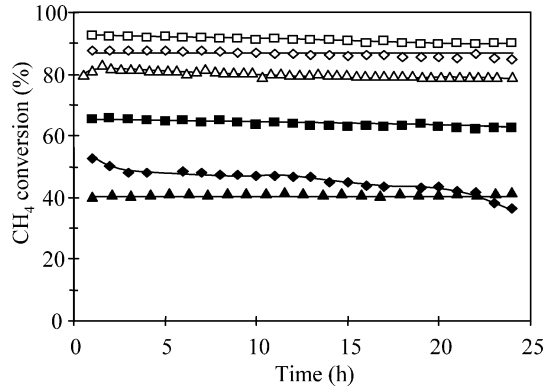


Fig. 10. $CH_4$ conversions vs time on stream for catalysts at 773 K (closed symbols) and 1073 K (opened symbols) (reaction condition: $CH_4/O_2/Ar/H_2O = 2/1/4/2$; SV = $1.7 \times 10^3$ l/(h g)). (◇,◆) Ni/MgAl-2, (□,■) NiRh/MgAl, (△,▲) Rh/MgAl-1.

Table 4
Amount of carbonaceous species on the catalysts after the reaction

| Catalyst | Fresh (wt%) | After reaction for 24 h (wt%) | | | |
|---|---|---|---|---|---|
| | | Without $C_2H_6$ | | With $C_2H_6$ | |
| | | 773 K | 1073 K | 773 K | 1073 K |
| Ni/MgAl-2 | 0.4[a] | 1.1[b] | 0.5[b] | 0.9[b] | 0.4[b] |
| NiRh/MgAl | 0.6[a] | 1.0[b] | 0.8[b] | 1.0[b] | 0.7[b] |
| Rh/MgAl-1 | 0.2[a] | 1.1[b] | 1.4[b] | 0.9[b] | 0.6[b] |
| SiC | 0.8 | | | | |

Reaction conditions: $CH_4/O_2/Ar/H_2O = 2/1/4/2$ or $CH_4/C_2H_6/O_2/Ar/H_2O = 1.6/0.2/1.4.2/2$; $1.7 \times 10^3$ l/(h g), 1073 or 773 K, 10 $mg_{cat}$.
[a] Without SiC.
[b] With 400 mg SiC.

with SiC did not show activity at both temperatures. At 1073 K, all catalysts exhibited stable activity during the period studied.

At 773 K the differences in the catalytic behavior were more pronounced. Specifically, the $CH_4$ conversion over NiRh/MgAl was much higher than that over Rh/MgAl-1, although both catalysts were stable. On the other hand, the initial $CH_4$ conversion over Ni/MgAl-2 was relatively high, but gradually decreased to 66% of the initial value with time on stream. The color of used Ni/MgAl-2 at 773 K was slightly greenish compared to gray color of the reduced material.

The concentrations of carbonaceous species on the catalysts after the reaction for 24 h are compiled in Table 4. The $CO_2$ evolving from the fresh sample is attributed to carbonates, which may also give a minor contribution to the $CO_2$ evolving from the used samples. Additionally, a small part of the $CO_2$ formed during TPO could also originate from SiC. Therefore, we conclude that the concentrations of deposited coke were small for all catalysts demonstrating strong resistance against coke deposition under the conditions studied.

### 3.8. Catalytic activity of catalysts in the presence of additional ethane

To study influence of light paraffins in natural gas, the flow rate of $CH_4$ in the above experiments was reduced to 80 vol% and 50 vol% of the reduced $CH_4$ was replaced by $C_2H_6$ (total concentration of carbon in the feed was kept constant). The Ar flow was increased to maintain the SV at $1.7 \times 10^3$ l/(h g). Note that the blank test with 400 mg SiC showed 63% conversion of $C_2H_6$, i.e., 12.6% of total conversion of hydrocarbons (normalized to the carbon number), at 1073 K, and around 60% of the converted $C_2H_6$ was dehydrogenated to $C_2H_4$. On the other hand, $C_2H_6$ conversion was not observed at 773 K. Conversions of $CH_4$ and of $CH_4$ and $C_2H_6$ are shown in Figs. 11A and B, respectively. $CH_4$ conversions in $CH_4/C_2H_6/O_2/Ar/H_2O$ condition were comparable to those in $CH_4/O_2/Ar/H_2O$ at both temperatures. On the other hand, the total conversions of the hydrocarbons in the former reactions were higher than $CH_4$ conversions in the latter reactions. Note that trace amounts of $C_2H_4$ (less than 1% yield) were also detected during the reaction at 1073 K. At both temperatures, $CH_4$ and total hydrocarbon conversions were very stable for most catalysts, except for Ni/MgAl-2 at 773 K for which the activity decreased slightly to 90% of its initial value. It should be noted that the decrease was less pronounced compared to the decrease with $CH_4/O_2/Ar/H_2O$ (Fig. 10).

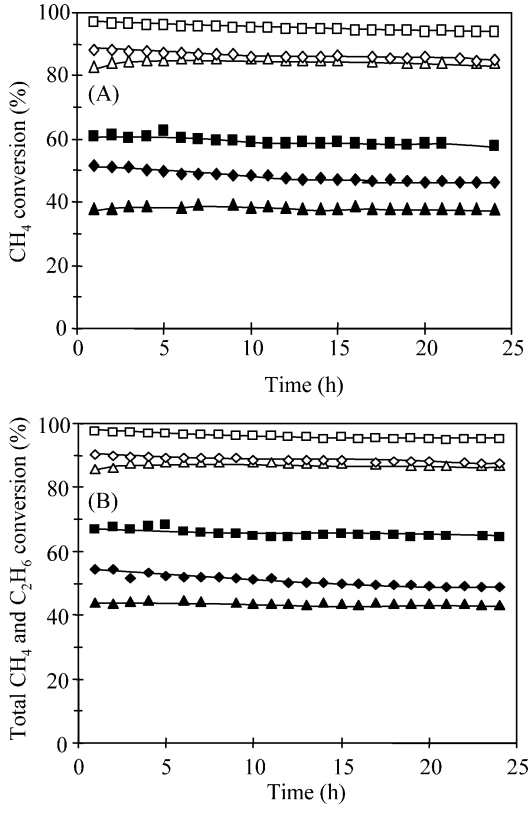


Fig. 11. (A) $CH_4$ conversions and (B) total $CH_4$ and $C_2H_6$ conversion (normalized by carbon number) vs time on stream for catalysts at 773 K (closed symbols) and 1073 K (opened symbols) (reaction conditions: $CH_4/C_2H_6/O_2/Ar/H_2O = 1.6/0.2/1/4.2/2$; SV $= 1.7 \times 10^3$ l/(h g)). (◇,◆) Ni/MgAl-2, (□,■) NiRh/MgAl, (△,▲) Rh/MgAl-1.

After the reaction for 24 h on the catalysts, the amounts of carbonaceous species are determined and compiled in Table 4. As the amounts of deposited coke were insignificant for all catalysts at both temperatures, we conclude that the catalysts also do not produce coke in the presence of ethane.

## 4. Discussion

### 4.1. Bulk and surface composition of the metal particles

The bulk and surface structures of metals of Ni/MgAl-2, Rh/MgAl-1 and NiRh/MgAl after the $H_2$ reduction at 1073 K are important to understand the catalytic properties. The $H_2$ uptake revealed that the metal surface area of Ni/MgAl-2 increased by a factor of 1.7, when approximately 2% of Ni were substituted by Rh (Ni/Rh = 49 molar ratio) (Table 1).

The XANES and the EXAFS at the Ni *K*-edge of Ni/MgAl-2 and NiRh/MgAl (Figs. 2 and 3) were very similar and revealed that Ni was not completely reduced after the $H_2$ treatment at 1073 K for 1 h (Table 2) in both catalysts. From the intensity of the maximum above the absorption edge a fraction of unreduced Ni species of about 20% was estimated. Significant differences in the EXAFS of NiRh/MgAl and Rh/MgAl-1 at the Rh *K*-edge were observed. The analysis of the EXAFS indicated that Rh–Rh contributions were essentially absent in the bimetallic catalysts (NiRh/MgAl), while strong Rh–Ni contributions were observed. The results indicate that (similar to PtNi [24]) a strong driving force exists to form a RhNi alloy and hence all reduced Rh atoms are surrounded by Ni (Table 3). It is interesting to note that Ni–Rh contributions were not observed at the Ni *K*-edge, which is attributed to very low loading of Rh compared to Ni, i.e., 0.89 wt% vs 25 wt%. Under these conditions the Rh atoms are located as isolated atoms and surrounded only by Ni atoms in the bimetallic RhNi phase. In contrast, most Ni atoms are surrounded by other Ni atoms in the bimetallic catalyst as only a very small fraction of Rh atoms are present, preventing to observe the Ni–Rh contribution within the limits of accuracy.

The degree of reduction estimated from the Rh–O contribution of Rh was much higher in NiRh/MgAl than in Rh/MgAl-1, which indicates that the presence of Ni drastically enhances also the reduction of Rh. The degree of reduction of the more abundant Ni species was hardly influenced by the presence of Rh, but gave an additional thermodynamic driving force for the presence of reduced Rh (dispersion in Ni). This shows that the degree of oxidation of Rh in Rh/MgAl-1 or Rh/MgAl-1 is not driven by the kinetics of reduction, but by the thermodynamics in the final material. It cannot be estimated at the moment in how far encapsulation of metal (oxide) particles by the oxidic support plays an important role.

Whatever the mechanism of the formation of the metallic particles may be, Ni and Rh oxide species are initially well dispersed in the oxidic precursor after calcination at 1173 K [8–10,27]. During the reduction process a relatively high mobility of Rh and Ni atoms must exist and the mutual influence (with the formation of the alloy as strong driving force) leads to the formation of particles in which Rh initiates the reduction of Ni (by increasing the availability of H atoms), but is also separated more clearly from the support, as the decrease in the Rh–O contribution in EXAFS clearly demonstrates. The presence of Rh, on the other hand, seems to provide anchoring of Ni and, therefore, results in smaller crystal size of Ni in NiRh/MgAl than that in Ni/MgAl-2 (Table 1).

The intensity of the band of linearly adsorbed CO was initially (2–4 min) stronger than that of bridged bonded CO for NiRh/MgAl. This tendency was reversed after the time indicating that CO at first adsorbs on Rh atoms. With time, however, the relative concentration of CO on Rh decreased, because Ni is the most abundant surface metal atom.

The particle size and the fraction of metal exposed were probed by three independent ways, i.e., TEM, $H_2$ chemisorption and XRD (see Table 1). The particle size was not determined by EXAFS, as the materials studied include reduced and oxidized metals making it, thus, ambiguous to determine realistic coordination numbers. The comparison of the size of the particles and hydrogen chemisorption (fraction of metal atoms that are at the surface) suggests an average degree of dispersion of 4.1 and 6.5% for Ni/MgAl-2 and NiRh/MgAl, respectively. The dispersion suggested by this method is lower than the values determined by XRD analysis by assuming spherical metal crystallites [28], i.e., 11.7 and 14.7% for Ni/MgAl-2 and NiRh/MgAl, respectively. We speculate that the difference points to a partial encapsulation of metal particles by the supports during the reduction.

### *4.2. Catalyst properties and behavior in $CH_4/O_2/Ar/H_2O$ reaction*

Catalyst deactivation is a significant issue in $CH_4$ autothermal reforming with high severity. It is caused by the decrease of catalytically active sites by coking, oxidation or sintering of the metal. The influence of such factors markedly depends on the reaction temperature and the operation severity. Deposited coke originates mainly from two reactions, i.e., $CH_4$ decomposition and CO disproportionation. The former is endothermic and favored at higher temperatures, while the latter is exothermic and favored at lower temperatures. Oxidation of metal may occur easily at lower temperatures at which methane cannot be activated [29,30]. On the other hand, sintering of metal particles is facilitated by higher temperatures. Operation severity in the laboratory mainly varied with the space velocity (SV), which is another important factor. Oxidative ($H_2O$, $O_2$, $CO_2$) and reductive ($CH_4$, CO, $H_2$) species are present during $CH_4$ autothermal reforming, i.e., low and high $CH_4$ conversions lead to atmosphere being oxidative and reductive, respectively. In order to operate the reformer with high efficiency, it is important to understand the catalytic behavior under the changing conditions.

In contrast to the similar catalytic stabilities of Rh/MgAl-1 and NiRh/MgAl in different SVs, the stability of Ni monometal catalysts was drastically changed by varying SVs (Fig. 9). To understand catalytic behavior of Ni monometal catalysts, we characterized Ni/MgAl-1 extensively. The catalyst showed high $CH_4$ conversions at 1073–873 K at the SV of $1.7 \times 10^2$ l/(h g) (Fig. 9C). However, the activity vanished at 773 K and the color of the used catalyst was greenish. XRD analysis of this material revealed that diffraction peaks of metallic Ni (observed after the $H_2$ reduction) disappeared completely, indicating that the inactivity was related to the oxidation of Ni in line with the color change. Note that the amount of carbonaceous species was insignificant, i.e., 0.2% including carbonates, after the reaction at 773 K. Activity can be restored by increasing the reaction temperature (Fig. 9C). This increase leads to the consumption of oxygen of NiO in oxidizing part of $CH_4$, which leads to reduced Ni and a more reducing atmosphere. The reduced Ni is able to catalyze $CH_4$ combustion and subsequent reforming to synthesis gas. Thus, metal oxides are more likely reduced at the outlet of the reactor than at the inlet. It is speculated that all metals were not reduced sufficiently by the reactants, if reduced Ni were once oxidized. This phenomenon would give the catalyst lower activity after re-reduction and greenish and gray colors at the inlet and outlet, respectively. Thus, we conclude that the increase of SV and decrease of the temperature leads to oxidation of Ni explaining the rather low activity at the higher SVs of both Ni monometal catalysts. Higher concentration of exposed Ni in Ni/MgAl-2 than Ni/MgAl-1 obviously contributes to suppress the deactivation due to the oxidation.

Rh monometal catalysts, on the other hand, showed very stable activity with varying temperature and SV (Fig. 9). Note that even if Rh/MgAl-1 was used at the SV of $1.2 \times 10^4$ l/(h g), the catalyst did not deactivate. Similar activities between Rh/MgAl-1 and Rh/MgAl-2 may be attributed to the lower Rh dispersion in Rh/MgAl-2 resulting from the higher Rh loading.

The oxidation of Ni was suppressed efficiently by the addition of small amounts of Rh (Ni/Rh = 49 in molar ratio). Two explanations of the role of Rh in retarding the oxidation of Ni are possible. One is related to the high catalytic activity (higher intrinsic activity) and because of the larger concentrations of metals exposed (factor of 1.7), which leads to more reductive atmosphere. Another possibility is presence of spillt-over H atoms from Rh to NiRh alloy particles [31]. By TPR, it was shown that reduction of Ni in Ni/MgAl-2 occurred at lower temperature by addition of small amounts of Rh (Fig. 7). Note that such enhancement of Ni reduction by noble metal has been attributed to hydrogen spillover from noble metal surface. However, also the oxidation of metallic Ni was promoted by Rh (Fig. 8). The nature of the bimetal-

lic alloy must be important for retarding the oxidation of Ni. While NiRh/MgAl showed slight deactivation at the very high SV ($1.2 \times 10^4$ l/(h g)) presumably through oxidation of the metal, its catalytic activity was significantly higher than that of Rh/MgAl-1 under all conditions studied (Fig. 10). Note that the slight deactivation can be suppressed by the introduction of a higher fraction of Rh.

### 4.3. Relevance of catalytic behavior in $CH_4/O_2/Ar/H_2O$ and $CH_4/C_2H_6/O_2/Ar/H_2O$ reaction

Total hydrocarbon conversions of Ni/MgAl-2, NiRh/MgAl and Rh/MgAl-1 were higher in $CH_4/C_2H_6/O_2/Ar/H_2O$ reaction (Fig. 11) than $CH_4/O_2/Ar/H_2O$ reaction (Fig. 10). This tendency is associated to the very high conversions of $C_2H_6$ (above 94% at 1073 K and above 58% at 773 K).

In both reactions, most of the catalysts were stable, except for Ni/MgAl-2 which gradually deactivated at 773 K. However, the deactivation was apparently suppressed by the partial replacement of $CH_4$ by $C_2H_6$. After the $CH_4/O_2/Ar/H_2O$ reaction, the catalyst was slightly greenish and the amount of carbonaceous species accumulated during the reaction was insignificant (Table 4). These results indicate the gradual deactivation can be ascribed to oxidation of Ni as discussed above. Faster consumption of oxidative species, $O_2$ and $H_2O$, induced by faster conversion of $C_2H_6$ than that of $CH_4$ helps retarding the oxidation of metallic Ni.

In general, thermal or steam cracking of the higher hydrocarbons can occur above 873–923 K even in the absence of the catalyst. The cracking leads to olefins followed by a carbonaceous polymer which can be dehydrogenated easily to produce coke deposition [32]. As part of $CH_4$ was replaced with $C_2H_6$, we speculate that carbonaceous deposition could be favored in $CH_4/C_2H_6/O_2/Ar/H_2O$ reaction. Especially, at 1073 K, a blank test revealed formation of $C_2H_4$ from $C_2H_6$ in the absence of the catalyst. Very low concentrations of $C_2H_4$ (less than 1%) were detected during the reaction in the presence of the catalysts. However, the amounts of carbonaceous species formed under the reaction conditions were insignificant, proving that catalysts prepared in this study had a strong resistance against coke deposition in autothermal reforming of natural gas. In addition, the observations suggest that ethane can be fully converted, while a large fraction of methane is still unconverted.

The coking tolerance of the catalysts is ascribed to the balance between the carbon forming and carbon consuming steps on the catalysts studied. The high concentration of oxidants in the reactants strongly assists for the carbon removing step. In addition, basic support (mixture of MgO and spinel) possibly dissociates water on metal support boundary and the reactive OH species can remove coke precursor from the metal particles [5].

## 5. Conclusions

Autothermal reforming of methane with or without $C_2H_6$ was carried out at 773–1073 K at the very high SV of ($1.7 \times 10^2$–$1.2 \times 10^4$ l/(h g)) over mono- and bimetal catalysts including Ni and/or Rh prepared from hydrotalcites. Higher loading of Ni contributed to prevent a low activity/inactivity due to oxidation of Ni metal. However, Ni/MgAl-2 including relatively large amount of Ni (26 wt%) also deactivated rapidly at the very high SV of $1.2 \times 10^4$ l/(h g). The deactivation was drastically retarded by the presence of Rh (Ni/Rh = 49). In NiRh/MgAl, reduction of Rh oxide species during $H_2$ pretreatment is enhanced by the presence of Ni. In turn Rh anchored NiRh alloy particles resulting in the formation of relatively small NiRh particles and higher fraction of metals exposed. A part of Rh is located at accessible sites on the NiRh alloy particles and contributes to maintain fully reduced Ni. On the other hand, Rh/MgAl showed very stable activity even at the very high SV, but its activity was lower than that of NiRh/MgAl under all conditions studied. These results suggest that catalyst compositions, SV and temperature gradient must be optimized carefully according to requirements of the system, i.e., operation condition and economical efficiency. Partial replacement of $CH_4$ by $C_2H_6$ increased conversion of total hydrocarbons and the more easy activation of $C_2H_6$ than $CH_4$ contributes to suppress oxidation of metal by consuming oxidative species in the reactant. It is possible with these catalysts also to selectively remove the higher alkane from methane by reaction. All catalysts prepared showed strong resistance for coke deposition in $CH_4$ autothermal reforming in the presence and absence of $C_2H_6$.

## Acknowledgments

K. Nagaoka acknowledges the Alexander von Humboldt foundation (Germany) for financial support. XAS experiments were carried out on the beamline X1 at HASYLAB, DESY, Hamburg, Germany which is supported by the EC by the IHP-Contract HPRI-CT-1999-00040/2001-00140. We thank Dr. Ayumu Onda for fruitful discussion. J.A. Lercher acknowledges support from the “Verband der Chemischen Industrie.”

## References

[1] J.A. Armor, Appl. Catal. 176 (1999) 159.
[2] M.A. Pena, J.P. Gomez, J.L.G. Fierro, Appl. Catal. A 144 (1996) 7.
[3] J.R. Rostrup-Nielsen, Catal. Today 71 (2002) 243.
[4] K. Takehira, T. Shishido, P. Wang, T. Kosaka, K. Takaki, J. Catal. 221 (2004) 43.
[5] J.R. Rostrup-Nielsen, in: J.R. Anderson, M. Boudart (Eds.), Catalytic Steam Reforming, Catalysis, in: Science and Engineering, vol. 5, Springer, Berlin, 1984.
[6] R. Vannby, S. Winter Madsen, Ammonia Plant Safety 32 (1992) 122.

[7] T. Hayakawa, H. Harihara, A.G. Andersen, A.P.E. York, K. Suzuki, H. Yasuda, K. Takehira, Angew. Chem., Int. Ed. Engl. 35 (1996) 192.
[8] F. Basile, L. Basini, G. Fornasari, M. Gazzano, F. Trifirò, A. Vaccari, Chem. Commun. (1996) 2435.
[9] F. Basile, G. Fornasari, E. Poluzzi, A. Vaccari, Appl. Clay Sci. 13 (1998) 329.
[10] F. Basile, L. Basini, M. D'Amore, G. Fornasari, A. Guarinoni, D. Matteuzzi, G. Del Piero, F. Trifirò, A. Vaccari, J. Catal. 173 (1998) 247.
[11] H. Morioka, Y. Shimizu, M. Sukenobu, K. Ito, E. Tanabe, T. Shishido, K. Takehira, Appl. Catal. A 215 (2001) 11.
[12] F. Basile, G. Fornasari, F. Trifirò, A. Vaccari, Catal. Today 64 (2001) 21.
[13] T. Shishido, M. Sukenobu, H. Morioka, M. Kondo, Y. Wang, K. Takaki, K. Takehira, Appl. Catal. A 223 (2002) 35.
[14] F. Basile, G. Fornasari, F. Trifirò, A. Vaccari, Catal. Today 77 (2002) 215.
[15] F. Basile, G. Fornasari, M. Gazzano, A. Kiennemann, A. Vaccari, J. Catal. 217 (2003) 245.
[16] F. Basile, G. Fornasari, V. Rosetti, F. Trifirò, A. Vaccari, Catal. Today 91 (2004) 293.
[17] T. Shishido, P. Wang, T. Kosaka, K. Takehira, Chem. Lett. (2002) 752.
[18] T. Shishido, M. Sukenobu, H. Morioka, R. Furukawa, H. Shirahase, K. Takehira, Catal. Lett. 73 (2001) 21.
[19] F. Cavani, F. Trifirò, A. Vaccari, Catal. Today 11 (1991) 173.
[20] H.P. Klug, L.E. Alexander, X-ray Diffraction Procedures, Wiley, New York, 1974.
[21] K.V. Klementiev, VIPER for Windows, freeware: http://www.desy.de/~klmn/viper.html;
K.V. Klementev, J. Phys. D: Appl. Phys. 34 (2001) 209.
[22] A.L. Ankudinov, J.J. Rehr, Phys. Rev. B 62 (2000) 2437.
[23] A.L. Ankudinov, B. Ravel, J.J. Rehr, S.D. Conradson, Phys. Rev. B 58 (1998) 7565.
[24] A. Jentys, B.J. McHugh, G.L. Haller, J.A. Lercher, J. Phys. Chem. 96 (1992) 1324.
[25] M. Primet, J.A. Dalmon, G.A. Martin, J. Catal. 46 (1977) 25.
[26] P.B. Rasband, W.C. Hecker, J. Catal. 139 (1993) 551.
[27] K. Takehira, Catal. Surv. Japan 6 (2002) 19.
[28] C.H. Bartholomew, R.B. Pannell, J. Catal. 65 (1980) 390.
[29] Y.-G. Chen, K. Tomishige, K. Yokoyama, K. Fujimoto, Appl. Catal. A 165 (1997) 335.
[30] A. Ayabe, H. Omoto, T. Utaka, R. Kikuchi, K. Sasaki, Y. Teraoka, K. Eguchi, Appl. Catal. A 214 (2003) 261.
[31] C. Raab, J.A. Lercher, J.G. Goodwin, J.Z. Shyu, J. Catal. 122 (1990) 406.
[32] S.H. Clarke, A.L. Dicks, K. Pointon, T.A. Smith, A. Swann, Catal. Today 38 (1997) 411.